REPORT DOCUMENTATION PAGE

Form Approved
OMB No. 0704-0188

PLEASE DO NOT RETURN YOUR FORM TO THE ABOVE ORGANIZATION.

1. REPORT DATE *(DD-MM-YYYY)*	2. REPORT TYPE	3. DATES COVERED *(From - To)*
29/04/2015	Journal Article	

4. TITLE AND SUBTITLE

A novel platform to study the effect of small-scale turbulent density fluctuations on underwater imaging in the ocean

5a. CONTRACT NUMBER

5b. GRANT NUMBER

5c. PROGRAM ELEMENT NUMBER

0602782N

6. AUTHOR(S)

Silvia Matt, Weilin Hou, Sarah Woods, Wesley Goode, Ewa Jarosz, Alan Weidemann

5d. PROJECT NUMBER

5e. TASK NUMBER

5f. WORK UNIT NUMBER

73-6604-04-5

7. PERFORMING ORGANIZATION NAME(S) AND ADDRESS(ES)

Naval Research Laboratory
Oceanography Division
Stennis Space Center, MS 39529-5004

8. PERFORMING ORGANIZATION REPORT NUMBER

NRL/JA/7330-14-2108

9. SPONSORING/MONITORING AGENCY NAME(S) AND ADDRESS(ES)

Office of Naval Research
One Liberty Center
875 North Randolph Street, Suite 1425
Arlington, VA 22203-1995

10. SPONSOR/MONITOR'S ACRONYM(S)

ONR

11. SPONSOR/MONITOR'S REPORT NUMBER(S)

12. DISTRIBUTION/AVAILABILITY STATEMENT

Approved for public release, distribution is unlimited.

13. SUPPLEMENTARY NOTES

14. ABSTRACT

Optical signal transmission is an important component of numerous underwater applications, including visibility and electro-optical (EO) communication, and may be limited by changes in the index of refraction due to small-scale variations in temperature and salinity associated with turbulence. The 2011 Bahamas Optical Turbulence Experiment (BOTEX) was conducted to investigate this underwater "optical turbulence". Our novel platform consisted of a high-speed camera and optical target mounted on a 5m-long frame, along with several Nortek Vector Acoustic Doppler Velocimeter and PME Conductivity -Temperature probes. Data on the background turbulence was collected with a Rockland Oceanographic Vertical Microstructure Profiler. This study was the first effort attempting to collect turbulence measurements on a frame designed for the investigation of "optical turbulence" in the ocean. Despite the numerous challenges, the investigation of the effect of microstructure on underwater optics is needed for efforts aimed at mitigating its impact on EO transmissions and may help advance optical methods to quantify oceanic microstructure.

15. SUBJECT TERMS

Underwater optics, Optical turbulence, In-situ measurements, Turbulence measurements

16. SECURITY CLASSIFICATION OF:			17. LIMITATION OF ABSTRACT	18. NUMBER OF PAGES	19a. NAME OF RESPONSIBLE PERSON
a. REPORT	b. ABSTRACT	c. THIS PAGE			Silvia Matt
Unclassified	Unclassified	Unclassified	UU	12	19b. TELEPHONE NUMBER *(Include area code)* (228) 688-5576

Reset

Standard Form 298 (Rev. 8/98)
Prescribed by ANSI Std. Z39.18

PUBLICATION OR PRESENTATION RELEASE REQUEST

14-1231-0859

Pubkey: 9508 NRLINST 5600.2

Ref: (a) NRL Instruction 5600.2
(b) NRL Instruction 5510.40D

Encl: (1) Two copies of subject paper (or abstract)

( ) Abstract only, published
( ) Book
( ) Conference Proceedings (refereed)
( ) Invited speaker
(X) Journal article (refereed)
( ) Oral Presentation, published
( ) Other, explain

( ) Abstract only, not published
( ) Book chapter
( ) Conference Proceedings (not refereed)
( ) Multimedia report
( ) Journal article (not refereed)
( ) Oral Presentation, not published

STRN NRLJA/7330-14-2108
Route Sheet No. 7330/
Job Order No. 73-6604-04-5
Classification X
Sponsor ONR BASE B02
approval obtained yes X no

Title of Paper or Presentation
Quantifying Optical Turbulence in the Open Ocean

Author(s) Name(s) *(First,MI,Last), Code, Affiliation if not NRL*

Silvia Matt NRC **Weilin Hou** 7333 **Sarah Woods** SPEC, Inc. **Wesley A. Goode** 7333 **Ewa Jarosz** 7332 **Alan D. Weidemann** 7333

It is intended to offer this paper to the _____
(Name of Conference)

(Date, Place and Classification of Conference)

and/or for publication in **Journal of Atmospheric and Oceanic Technology, Ur**
(Name and Classification of Publication) *(Name of Publisher)*

After presentation or publication, pertinent publication/presentation data will be entered in the publications data base, in accordance with reference (a).
It is the opinion of the author that the subject paper (is ____) (is not __X__) classified, in accordance with reference (b).
This paper does not violate any disclosure of trade secrets or suggestions of outside individuals or concerns which have been communicated to the Laboratory in confidence. This paper (does ____) (does not __X__) contain any militarily critical technology.
This subject paper (has ____) (has never __X__) been incorporated in an official NRL Report.

Weilin Hou, 7333 _____
Name and Code *(Principal Author)* (Signature)

CODE	SIGNATURE	DATE	COMMENTS
Author(s) Hou		3/11/14	Need by 04 Apr 14
			Publicly accessible sources used for this publication
			This is a Final Security Review. Any changes made in the document, after approved by Code 1231, nullify the Security Review.
Section Head Hou		3/11/14	
Branch Head Richard L. Crout, 7330		3-12-2014	
Division Head Ruth H. Preller, 7300		3/12/14	1. Release of this paper is approved. 2. To the best knowledge of this Division, the subject matter of this paper (has ____) (has never __X__) been classified.
Security, Code 1231		3/12/14	1. Paper or abstract was released. 2. A copy is filed in this office.
Office of Counsel,Code 1008.3	Kathy Chapman	3/18/14	
ADOR/Director NCST E. R. Franchi, 7000			
Public Affairs *(Unclassified/ Unlimited Only)*, Code 7030.4	Shannon Mercer	3-17-14	
Division, Code			
Author, Code			

12 MAR '14 PM3:01

HO-NRL 5511/6 (Rev. 12-88) (e) THIS FORM CANCELS AND SUPERSEDES ALL PREVIOUS VERSIONS

Methods in Oceanography 11 (2014) 39–58

Contents lists available at ScienceDirect

Methods in Oceanography

journal homepage: www.elsevier.com/locate/mio

Full length article

A novel platform to study the effect of small-scale turbulent density fluctuations on underwater imaging in the ocean

Silvia Matt [a,*], Weilin Hou [b], Sarah Woods [c,1,2], Wesley Goode [b], Ewa Jarosz [b], Alan Weidemann [b]

[a] National Research Council Research Associate at Naval Research Laboratory, 1009 Balch Blvd, Stennis Space Center, MS 39529, USA

[b] Naval Research Laboratory, 1009 Balch Blvd, Stennis Space Center, MS 39529, USA

[c] SPEC Inc., Boulder, CO, USA

ARTICLE INFO

Article history:
Received 16 August 2014
Received in revised form
12 January 2015
Accepted 20 January 2015

Keywords:
Underwater optics
Optical turbulence
In-situ measurements
Turbulence measurements

ABSTRACT

Optical signal transmission is an important component of numerous underwater applications, including visibility and electro-optical (EO) communication. In addition to the well-studied effect of particle backscatter, underwater optical signal transmission can be limited by changes in the index of refraction (IOR) due to small-scale variations in temperature and salinity, sometimes called "optical turbulence". These variations in IOR, which are associated with oceanic turbulence, can lead to the blurring of an underwater optical target, particularly at high spatial frequencies, thus reducing target detail. The 2011 Bahamas Optical Turbulence Experiment (BOTEX) was conducted to investigate this impact of turbulence on underwater optical signal transmission. Investigating naturally occurring "optical turbulence" requires a platform held at depth, capable of concurrent measurements of optical impairment by turbulence, which requires a significant optical path length, as well as associated physical and optical background conditions of the ambient environment. Our novel platform consisted of a high-speed camera and optical target mounted on a 5*m*-long frame, along with several Nortek Vector Acoustic Doppler Velocimeter (ADV) and PME Conductivity–Temperature (CT) probes, to estimate

* Corresponding author.
E-mail address: silvia.matt@nrlssc.navy.mil (S. Matt).

1 Primary affiliation: NRL ASEE Postdoctoral Fellow.

2 Now at: SPEC Inc., Boulder, CO, USA.

http://dx.doi.org/10.1016/j.mio.2015.01.001
2211-1220/Published by Elsevier B.V.

turbulent kinetic energy and temperature variance dissipation rates experienced by the frame. Data on the background turbulence was collected with a Rockland Oceanographic Vertical Microstructure Profiler, to aid in analysis and guide error estimates of the ADV/CT measurements. This study was the first effort attempting to collect turbulence measurements on a frame designed for the investigation of the effect of density microstructure variations on optical signal transmission in the open ocean. Our results highlight the numerous challenges associated with studying this phenomenon in the dynamic oceanic environment. Here, we present the interpretation of the high-resolution velocity and temperature measurements collected on the frame and discuss the associated difficulties. Despite the numerous challenges, the investigation of the effect of microstructure on underwater optics is needed for efforts aimed at mitigating the impact of "optical turbulence" on underwater EO signal transmission and may help advance optical methods to quantify oceanic microstructure.

Published by Elsevier B.V.

1. Introduction

Optical properties of coastal and open ocean water and their impact on electro-optical (EO) imagery are important for a wide range of applications. Diver visibility, mine detection, search and rescue, and optical communications all depend on underwater optical signal transmissions. Underwater imaging has been shown to be affected by absorption and scattering due to suspended particles (Hou et al., 2007). However, recent evidence suggests that, in addition to particle scattering, underwater EO imagery may also be significantly affected by turbulent temperature and salinity microstructure in the water. Turbulence is ubiquitous in the world's oceans and fresh-water environments and the associated small-scale temperature and salinity variations can lead to localized changes in the index of refraction, which in turn impacts underwater optical properties. It has been demonstrated that this so-called "optical turbulence" can be a limiting factor in natural environments, affecting optical signal transmission that impact various applications, from diver visibility to active and passive remote sensing (Hou et al., 2012b; Bogucki et al., 2004). The recent Skaneateles Optical Turbulence Experiment (SOTEX) conducted in a lacustrine environment confirmed that optical turbulence may significantly contribute to image degradation (Hou et al., 2012b; Woods et al., 2011). To quantify this impact of turbulence on optical signal transmission in an oceanic environment, the Bahamas Optical Turbulence Experiment (BOTEX) was conducted in the summer of 2011 (Fig. 1) (Hou et al., 2012a). Measuring turbulence in the ocean has long been known to be a challenging task, and thus studying naturally-occurring optical turbulence in the open ocean is rife with difficulties. Among these are the deployment strategy, as well as ambient atmospheric and oceanographic conditions that can also affect the measurement method. The goal of this paper is to describe and address the challenges encountered while working to measure turbulence parameters with an experimental array that is geared towards optics measurements and different from the traditional turbulence profiling or fixed mooring approach. Since turbulence is patchy and highly variable in both space and time, it is important to have a type of turbulence sensor on the same structure that is also measuring information on the optics. This limits what turbulence sensors can be used. Shear probes, such as used in traditional Vertical Microstructure Profilers (VMP) and generally deployed at a free-fall from the vessel, would not be useful on a tethered frame drifting with the boat. The requirements on optical path length further complicate the setup. An optical path length of several meters is desirable in particle-laden natural waters, since the effect of image distortion due to turbulence is cumulative and often less pronounced than that of blurring due to particle scattering (Duntley, 1963; Preisendorfer, 1986; Hou et al., 2007). This puts certain size requirements on the frame to measure the optics, which in turn limits the ability to let

Fig. 1. Location of stations during BOTEX.

the array free-fall through the water column. In the present study, we settled on the use of Acoustic Doppler Velocimeters (ADVs) and high-resolution thermistors (PME Conductivity–Temperature (CT) probe) affixed to the frame. However, the use of ADVs to infer turbulent kinetic energy dissipation rates (TKED) is known to be inherently more successful in more energetic environments. In more quiescent waters, the signal to noise ratio of the sensor may reach its lower limit. Since noise from platform motion and vibrations can complicate the estimation of turbulence properties from the ADV/CT package, complementary measurements of ambient turbulence levels with a dedicated microstructure profiler, such as the VMP, are an invaluable tool to aid in data analysis and guide error estimates.

This paper describes our instrument setup, the procedures used to calculate turbulence parameters from the measurements, as well as the challenges encountered with our system. We also briefly discuss the concurrent optical observations and their relation to the observed turbulence parameters. A more detailed analysis of the optical measurements taken during this field experiment will be the subject of future work.

2. Methods

The goal for the measurements obtained during this study was to be able to image across a significant optical path length while at the same time collecting data on the turbulence properties of the ambient water. Deploying a free-falling platform similar to a traditional turbulence profiler would severely limit the optical path length and hinder the ability to image across naturally occurring optical turbulence, such as in the thermocline. Imaging across such naturally occurring density variations in index of refraction (IOR) is, of course, also complicated if the frame is tethered to a drifting vessel and affected by cable motion and vibrations, where the frame itself may induce turbulence. The approach chosen was a compromise, providing a significant optical path length along the measurement structure – a 5 m long, rigid aluminum frame, termed the Image Measurement Assembly for Subsurface Turbulence (iMast), – while simultaneously collecting high-resolution velocity and temperature data for estimation of turbulent properties of the water. A similar frame was used during the same field exercise to study laser sensing of mixed layer turbulence (Dalgleish et al., 2013), however, these measurements did not collect any turbulence data directly on the frame, but rather compared the optics results to the background values from the VMP. Depending on sea state and atmospheric conditions, as well as due to the patchy and time-variable nature of turbulence, such an approach omits an important piece of information, the turbulence encountered at the time of the optical measurements, as well as frame-induced turbulence.

Thus, in order to characterize the velocity and temperature microstructure experienced by the optics on our frame, high-resolution velocity and temperature measurements were obtained with

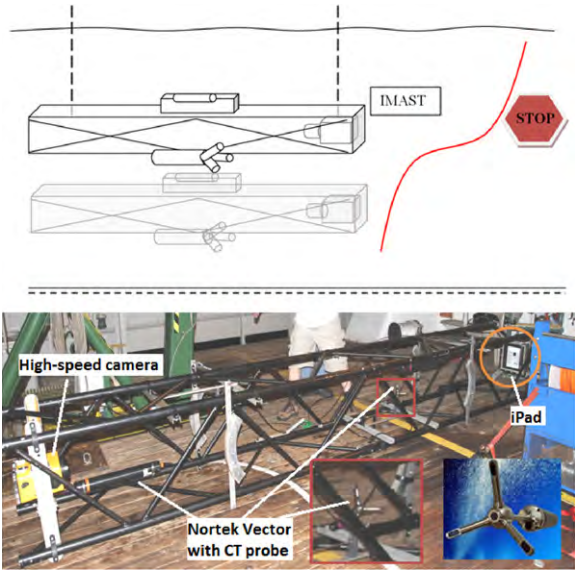

Fig. 2. Schematic of iMast deployment during BOTEX (top) and photograph of iMast on deck showing the ADV/CT probes mounted on the frame, the high-speed camera and the iPad as optical target (bottom).

a Nortek Vector Acoustic Doppler Velocimeter (ADV) and PME Conductivity–Temperature (CT) microstructure probe simultaneously with measurements of optical target clarity, i.e., a high-speed camera was continuously imaging an optical target across a region of turbulence or quiescent water. Since turbulent properties from the ADV/CT data are difficult to estimate and are sensitive to contamination by platform and cable motion, background turbulence levels were also assessed with a traditional turbulence profiling instrument. This Vertical Microstructure Profiler (VMP) measures velocity shear and temperature while freely falling through the water column (VMP is manufactured by Rockland Oceanographic Services Inc., Canada and similar to a profiler described in Wolk et al., 2002). The TKED and temperature variance dissipation rates (TD) were calculated from the ADV/CT measurements via spectral fitting to Kolmogorov spectra (for velocity) and Batchelor spectra (for temperature) and compared to TKED and TD estimates from the VMP (Oakey, 1982).

2.1. Data collection

The ADV and CT probes, along with a high-speed imaging camera on one end and optical targets (active and passive) on the other, were mounted on the rigid aluminum frame of the iMast. The iMast structure was deployed from the R/V Walton Smith's A-frame and lowered to a set of predetermined depths (Fig. 2) (Hou et al., 2012b). The frame, tethered to the ship, was held at these depths for 10–15 min long "depth pauses", to collect time series of high-resolution velocity and temperature/conductivity for the subsequent estimation of TKED and TD rates. Data were collected at a sampling frequency of 32 Hz. The pauses were taken at depths where optical turbulence associated with strong temperature gradients was expected to be most pronounced, i.e. at the bottom of the mixed layer and just below the thermocline, although results from the study using a longer frame during the same field experiment showed significant cumulative effects across most of the upper layer (Dalgleish et al., 2013). For comparison, additional data were collected at depths exhibiting low temperature variability. The estimation of TKED and TD from this tethered structure is complicated by platform movement, and hence additional data on the background turbulence was collected with the VMP either immediately preceding or succeeding the iMast deployment. These measurements to describe the ambient turbulence levels were taken with a Rockland VMP, which was deployed as a free-falling profiler loosely tethered to the ship. In this paper, we focus on the data collected with the iMast;

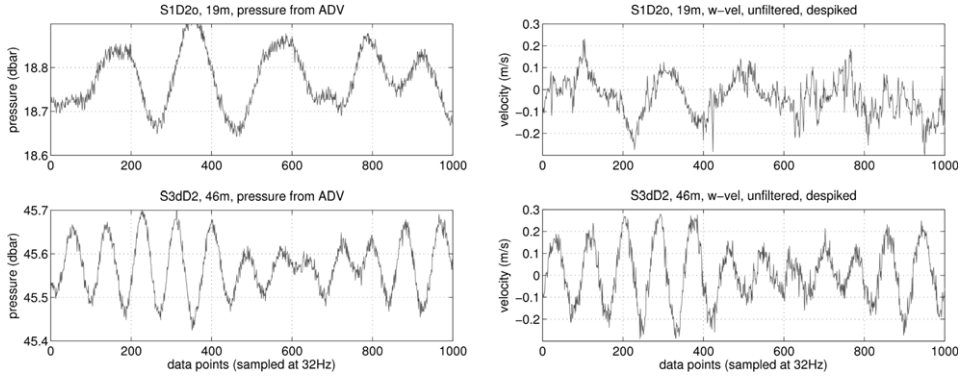

Fig. 3. Pressure (left) and velocity (right) time series from the Florida coast (Station 1, top) and the Bahamas (Station 3d, bottom) illustrate platform motion felt by the ADV/CT probes on the iMast. The extent of vertical movement by the frame is similar at both stations, but the period of motion is shorter and the vertical velocities are higher at the Bahamas station. Meteorological conditions were recorded as calm at Station 1 (yet with strong currents and drift), and as rougher with pronounced swell at Station 3.

data collection with the VMP and processing of its data follow established protocols, more details can be found in Oakey (1982) and Hou et al. (2012b). In addition to the measurements of turbulent properties, hydrographic and optical properties of the water were measured with a SeaBird Conductivity–Temperature–Depth (CTD) and a WetLabs ac-9 transmissometer mounted on a small wire cage and deployed from the vessel at each station before or after the iMast or VMP deployments.

2.2. Calculation of TKED and TD

2.2.1. Turbulent kinetic energy dissipation rate—TKED

The estimation of TKED rates from velocity time series collected with ADVs is based on the well-established Inertial Subrange Dissipation Method (IDM) (see, f. ex., Bluteau et al., 2011) and is based on fitting observed velocity spectra to the theoretical energy spectrum of turbulence described by Kolmogorov (see, f.ex., Lesieur, 2008), which exhibits a $-\frac{5}{3}$ slope in the inertial subrange (ISR). The spectral fitting requires that an ISR is present and well-resolved in the spectra. Deployment strategies thus have to take into account platform motion and instrument configuration, as these can introduce motion that may cause contamination of the ISR of the spectrum (Fig. 3). Resolving the ISR also puts a minimum requirement on the record length. Ideally, the full 10–15 min time series from the depth pauses would be used to calculate TKED. However, excessive noise in the data due to platform vibrations as well as directional changes in mean flow U often reduced the length of usable data segments.

Spectra were calculated from velocity time series, and Taylor's Frozen Turbulence hypothesis (see, f. ex., Tennekes and Lumley, 1972), $k = \frac{2\pi f}{U}$, is applied to convert the frequency spectra to wavenumber spectra. Here, k is the wavenumber (in rad m^{-1}), f is the frequency (in s^{-1}), and U is the mean flow past the sensor (in m s^{-1}). A wavenumber range representative of the spectrum in the ISR is chosen and the TKED rate ϵ is estimated from

$$E_{ii}(k_1) = C\epsilon^{\frac{2}{3}} k_1^{-\frac{5}{3}}, \tag{1}$$

where

$$\int_0^\infty E_{ii}(k_1)\, dk_1 = \bar{u}_i^2. \tag{2}$$

Here, E_{ii} is the one-dimensional velocity spectrum of component i ($x_1 = x$ is the streamwise component, $x_2 = y$ is the transverse component, and $x_3 = z$ is the vertical component, in a Cartesian coordinate system), and $\bar{u}_i^2$ is the variance of the signal. C is a constant equal to $\frac{18}{55}\alpha$

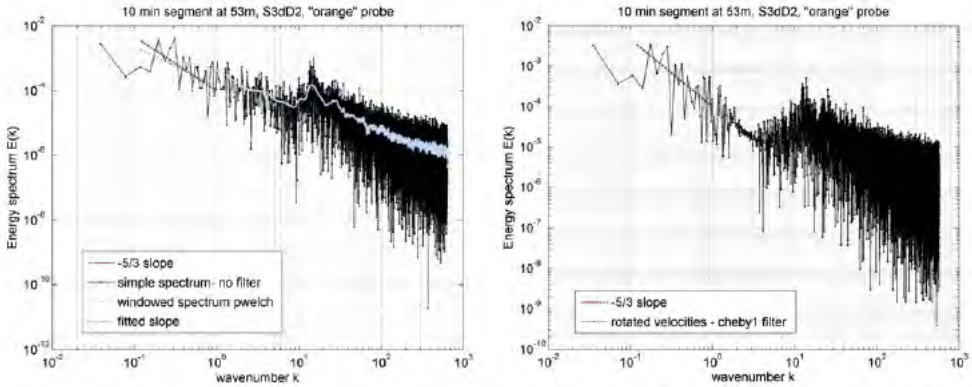

Fig. 4. Energy spectra from the streamwise velocity component at Station 3 in the Bahamas (Tongue of the Ocean). Note the peak at wavenumber $k \approx 10$–20 rad/s (corresponding to a period of about 3–5 s) in the unfiltered spectra (left), which is due to ship/platform motion. For the spectrum shown on the left, U was chosen to be the larger of the horizontal velocity components. The filtered spectrum is shown on the right. Here, the velocities were rotated into a new frame of reference with $\overline{U} = (\overline{U}_1, 0, 0)$. The slope in the inertial subrange of the spectra is in agreement with the Kolmogorov $-\frac{5}{3}$ law.

in the streamwise direction (x and k_1) and to $\frac{4}{3}\frac{18}{55}\alpha$ in the transverse or vertical direction (y, z); $\alpha \approx 1.5$ is the Kolmogorov constant (e.g., Rusello and Cowen, 2011). Since a considerable source of uncertainty in the estimation of ϵ is introduced through the choice of the mean flow U for the application of Taylor's Frozen Turbulence hypothesis, we follow Bluteau et al. (2011) and rotate our observed velocities (which were collected in XYZ-coordinates, the coordinate system of the sensor, then rotated into geophysical coordinates) into a new frame of reference where $\overline{U} = (\overline{U}_1, 0, 0)$ (Bluteau et al., 2011). $\overline{U}_1$ is then used in the conversion from frequency to wavenumber space. For our data, the wavenumber range to fit to the theoretical spectrum was chosen manually, we found this approach to yield a more robust result than automating the routine, especially in the case of noisy spectra (Fig. 4). The fit to the data was accomplished by using the approach introduced by Bluteau et al. (2011), based on a maximum likelihood estimator (MLE) technique, previously used for Batchelor spectral fitting (Ruddick et al., 2000). This approach also allows the estimation of errors on TKED through the MLE method as described in Bluteau et al. (2011) and Ruddick et al. (2000). These errors represent the quality of the fit of the observed spectrum to the theoretical $-\frac{5}{3}$ slope. They do not, however, adequately describe all uncertainties present in the data due the assumptions underlying the Frozen Turbulence Hypothesis and ISR method.

One issue that arose in our data was the occurrence of so-called "phase-wrapping", which can occur if the ambient velocity exceeds the maximum velocity that can be measured by the instrument, the so-called ambiguity velocity. This maximum measurable velocity of the ADV is determined by an instrument setting controlling the pulse separation, the nominal velocity range, and applies to the beam velocities (Fig. 5). Generally, it should be ensured that the ambiguity velocity is not exceeded during deployment, however, this increase in nominal velocity range, i.e., a decrease in pulse separation, also leads to a decrease in instrument resolution. Since this limit on measurable velocity applies to the beam velocities, phase-wrapping can occur even if the observed earth-referenced velocities do not exceed the estimated maximum velocity range (Rusello, 2009). Data with mild to moderate amounts of phase-wrapping can be corrected for in post-processing. The correction has to be applied for the beam velocities and requires a coordinate transformation if data is collected in XYZ or ENU coordinates (i.e., the coordinate system relative to the probe head or the geophysical coordinate system, respectively) (Rusello, 2009). Extreme cases of phase-wrapping can be too noisy to unwrap successfully and may introduce spuriously high values for TKED dissipation; such data were rejected in our analysis.

2.2.2. Temperature variance dissipation rate—TD

While we did collect conductivity data, we chose here to report only on the temperature data. It has previously been reported that variations in the index of refraction in the ocean are mainly driven

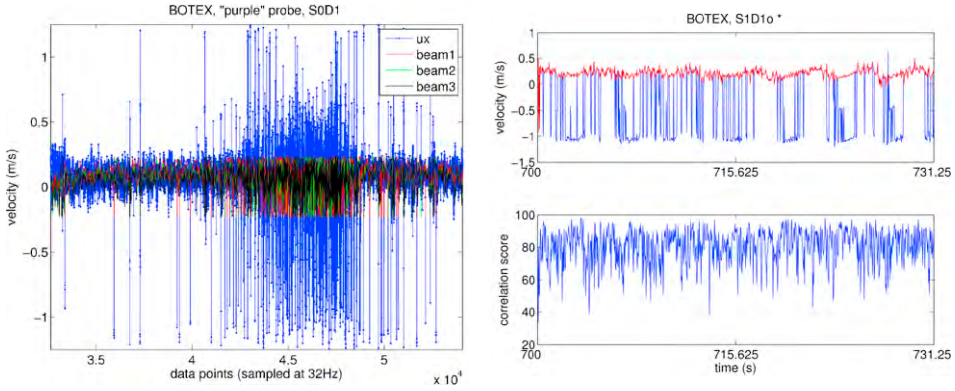

Fig. 5. Phase-wrapping occurs when the so-called beam ambiguity velocity, u_{amb}, is exceeded (for $|u_{amb}| > 0.23$ m/s in our case). This leads to spurious velocities in the probe- or earth-referenced data (left panel, blue line). The ambiguity velocity is determined by an instrument setting, which controls the pulse separation in pulse-coherent Doppler velocimeters. When data is phase-wrapped, the correlation score between successive pulses (should be >70%) drops (bottom right panel). Such data has to be rejected unless it can be corrected, i.e. "unwrapped". The red line in the top right panel shows the "unwrapped" velocity, the blue is the phase-wrapped data.

by temperature fluctuations (Bogucki et al., 1998, 2004). Furthermore, we felt that our conductivity data may not be reliable enough to properly estimate salinity variance dissipation rates, as described in Nash and Moum (1999), especially given our relatively low sampling frequency.

For the estimation of TD rates from the temperature time series, we followed Moum and Nash (2009), fitting temperature gradient spectra to the theoretical Batchelor spectrum. This technique involves fitting the temperature gradient spectra in the dissipative high-frequency range of the spectrum. To obtain temperature gradient spectra from the temperature time series, we again invoke Taylor's frozen turbulence hypothesis and use

$$\frac{dT}{dx} = \frac{1}{U}\frac{dT}{dt} \tag{3}$$

and $\hat{k} = f/U$ (note that $\hat{k}$ has units of cpm). For isotropic turbulence, the dissipation rate of the temperature variance can be described as

$$\chi_T = 6D_T\left\langle \frac{dT}{dx}\frac{dT}{dx}\right\rangle = 6D_T\int_0^\infty \Psi_{T_x}(k)\,dk, \tag{4}$$

where D_T is the thermal diffusivity, and $\Psi_{T_x}(k)$ is the wavenumber spectrum of $\frac{dT}{dx}$, the along path component of the temperature gradient (Moum and Nash, 2009). We then explored the use of MLE spectral fitting to our data (Ruddick et al., 2000). However, since our spectra do not resolve the high-frequency part of the spectrum (up to the Batchelor cut-off wavenumber k_B), the method described by Moum and Nash (2009) is more appropriate for our data. This approach is based on integrating the theoretical spectrum. For consistency, the data are again filtered for platform motion, which does however not affect the frequency range of the spectrum involved in the Batchelor fit. Furthermore, a spectral correction to the signal measured by the thermistor is applied through a single pole response function

$$H^2(\hat{k}) = \frac{1}{[1+(U\hat{k}/f_c)^2]}, \tag{5}$$

with $f_c = 20$ Hz (Moum and Nash, 2009; Bogucki et al., 2012). The correction is done by multiplying the spectra by the inverse of the filter function.

To ensure that U varies as little as possible over the segment used to calculate temperature gradient spectra, spectral estimates were done from 4-s data segments (128 data points) and the results for χ

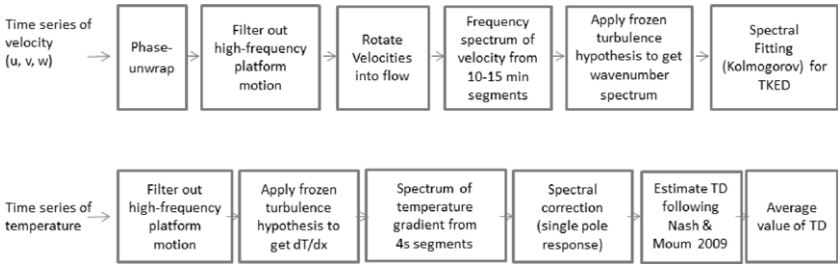

Fig. 6. Flowchart visualizing the processing steps used for calculation of TKED (top) and TD (bottom).

were averaged. The length of 4 s for the data segments was chosen as a trade-off between having an adequate number of points to calculate the spectra, while keeping the segment length as short as possible to limit variability of the mean flow. Our sampling frequency of 32 Hz is at least three to four times lower than that generally used to estimate χ from temperature measurements. Despite this shortcoming, which is due in part to the limitation of the temperature probe being integrated with and controlled by the ADV, we find the TD rates we obtain from either method to be robust. The calculated values of TD are consistent between data from different sensors at the same measurement time and depth, nonetheless, uncertainties are introduced in a number of ways (frame movement, choice of U, mean temperature gradient, among others), which cannot adequately be quantified at this point.

The Batchelor spectral fitting technique can also be applied to estimate ϵ, through the relationship

$$k_B = \left[\frac{\epsilon}{\nu D_T^2}\right]^{\frac{1}{4}}, \tag{6}$$

which ties the Batchelor wavenumber k_B to the TKED rate ϵ (ν is the molecular viscosity of water), as well as the relationship

$$\epsilon_\chi = \frac{N^2 \chi}{2\Gamma \left\langle \frac{dT}{dz} \right\rangle^2}, \tag{7}$$

where ϵ_χ signifies TKED derived from χ. Here, $\Gamma = 0.2$, N is the local buoyancy frequency, and $\langle \frac{dT}{dz} \rangle$, is the local temperature gradient, which can be estimated directly from our data following the procedure described in Moum and Nash (2009). The mean temperature gradient $\langle \frac{dT}{dz} \rangle$ is estimated from 1-min long data segments. Likely due to the fact that our spectra are severely under resolved in the range preceding k_B, as well as due to uncertainties associated with local estimates of $\langle \frac{dT}{dz} \rangle$ and N^2, we found our estimates of ϵ_χ from the temperature gradient spectra to be less robust than those of χ itself. The individual processing steps for TKED and TD are visualized in the flow chart shown in Fig. 6.

2.3. Optical measurements on the iMast

The velocity and temperature data on the iMast were collected in the context of optical target clarity and spatial resolution. A resolution chart was mounted to one side of the iMast, a high-definition camera to the other. Video of the optical chart were taken during the deployments and the images assessed for image degradation. The optical target used in this analysis was the image of an optical chart on an iPad screen, hence an active target. Only one pattern was used in this study (of the 1951 USAF resolution test chart type), but the setup with the iPad as active target allows the use of a variety of optical charts, including slant angle and grid patterns. The camera was a Casio EXILIM EX-F1, which saves video in MOV format, H.264/AVC standard. The videos were shot in different resolutions; near the Florida coast, the video was shot in High-Speed (HS) with 512 by 384 pixels at 300 frames per second (fps), while in the Bahamas, the video setting was High-Definition (HD), with 60 fps and resolution 1920 by 1080 pixels. Since the data collection was plagued by noise issues due to platform motion, as described above, these were the only two videos where we also had coinciding and usable

turbulence measurements. For subsequent image analysis, frames were extracted as TIFF images from the MOV videos. To quantify the extent of image degradation from optical turbulence, a common approach involving the Structural Similarity Index (SSIM) Method (Wang et al., 2004) was used. The SSIM method is an image quality metric and measures the similarity between two images, when one is considered the "perfect quality" reference image.

The SSIM value is calculated as the measure between two windows x and y of common size N by N as

$$SSIM(x, y) = \frac{(2\mu_x\mu_y + c_1)(2\sigma_{xy} + c_2)}{(\mu_x^2 + \mu_y^2 + c_1)(\sigma_x^2 + \sigma_y^2 + c_2)}. \tag{8}$$

Here, μ_x is the average of x, μ_y is the average of y, σ_x^2 is the variance of x, and σ_y^2 the variance of y. σ_{xy} is the covariance of x and y. $c_1 = (k_1 L)^2$ and $c_2 = (k_2 L)^2$ are variables, where L is the dynamic range of the pixel values and default values are for $k_1 = 0.01$ and $k_2 = 0.03$. The SSIM index then becomes a value between -1 and 1, where 1 is the value achieved for identical sets of data. A more detailed description of the method and comparison to other image metrics such as mean square error (MSE) and peak signal-to-noise ratio (PSNR) can be found in Wang et al. (2004). For our calculation,we used the Matlab script provided at "https://ece.uwaterloo.ca/~z70wang/research/ssim/ ".
To account for frame motion and vibration in the videos, successive images were image registered using "imregister" in Matlab's Image Processing Toolbox, which is an intensity-based image registration algorithm (see "http://www.mathworks.com/help/images/ref/imregister.html"). In addition to the SSIM, we also calculated the sum of absolute differences (SAD) for subsequent video frames. This simple method eliminates the need for a reference image. The value of SAD was then scaled to fit into the range 0–1 and, for comparison with SSIM, we calculated $1 - SAD$.

3. Results

3.1. TKED

We compare data from two stations, Station 1 near the Florida coast, on the shelf in an area influenced by the Gulf Stream, and Station 3d in the Bahamas, in a deep basin called the Tongue of the Ocean (Fig. 1). Repeat casts from the VMP near Station 1 reveal an energetic environment in the upper ocean, with TKED rates ϵ reaching as high as 10^{-5} m^2 s^{-3} in the top 20 m above the thermocline and around 10^{-7} to 10^{-6} m^2 s^{-3} in the thermocline (Fig. 7). The station was occupied for two days, June 30 and July 2, the VMP casts were taken on July 2. The differences in mixed layer depth and stratification between the two days can be explained by the temporal and spatial variability characteristic of this highly energetic area on the east Florida shelf, especially since the boat was drifting during deployments. The variability shown during successive VMP casts is also typical of such a deployment strategy, since the boat will drift in and out of strongly turbulent regions, which in themselves are intermittent and vary in both space and time. The TKED rates from the ADV on the iMast fall well within the range of the VMP measurements. The ADV data was clean enough for the estimation of ϵ at $\sim$20 m depth from all three ADVs on both days, and the values center around $\epsilon \approx 10^{-6}$ m^2 s^{-3}. Excessive noise and phase-wrapping in several probes at deeper depths led to fragmented data that did either not resolve the ISR or exhibited unrealistically high values of ϵ due to noisy velocity series. These data had to be rejected. The data from which ϵ could be calculated for the deeper pauses, at $\sim$27 m on June 30 and at $\sim$43 m on July 2 show that they fall within the range of values shown by the VMP. The large margin of error at around 27 m can also be attributed to high levels of noise and phase-wraps in the velocity data. The data from $\sim$10 m on June 30 show TKED values significantly lower that those of the VMP on July 2. This is not unexpected given the intermittent and spatially varying nature of turbulence, and can be explained by different wind conditions for the two days, affecting the mixing in the upper ocean, as well as spatial differences between cast locations taken from the drifting vessel. Estimates of TKED from the microstructure temperature data, ϵ_χ also mostly fall within the range of ϵ measured by the VMP and the ADVs on the iMast, but as explained in Section 2.2.2, they were considerably less robust than the values derived from the ADV measurements. Since the frame of the iMast is tethered to the drifting vessel, and affected by this drift, as well as

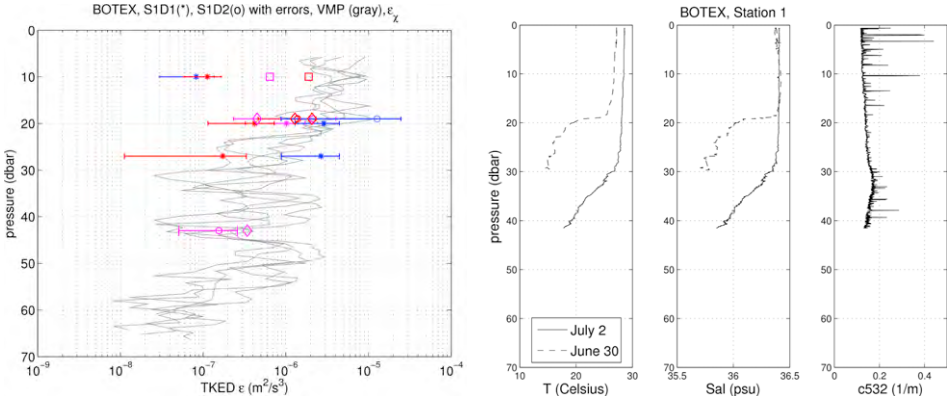

Fig. 7. TKED rates from Station 1 on the Florida coast from VMP and Nortek ADV on the iMast (left). The station was occupied on June 30 and July 2, 2011. Stratification and c532 from the CTD/optics package at this station are shown on the right. The thin lines show different realizations of VMP drops for ϵ on July 2. Estimates of TKED rate ϵ from the ADV data are shown as stars (June 30) and circles (July 2) with associated error bars (2 standard errors estimated via MLE technique). Individual points signify data from three different instruments, color-coded red, purple and blue. Diamonds (July 2) and squares (June 30) are estimates of ϵ_χ from temperature gradient spectra from the microstructure temperature probe on the iMast.

cable motion due to swell and vessel movement, the frame is expected to generate a non-negligible amount of turbulence while being dragged through the water. Thus, we would generally expect the values of turbulence parameters from the measurements on the iMast to be higher than or on the high end of those from the VMP, except for the case of very calm conditions, such as may be encountered in lakes or estuaries (Hou et al., 2012b). Nevertheless, it is important to be able to characterize the turbulence experienced by the optics on the iMast itself, and not merely compare the optics data to the background turbulence data from the VMP. The data we collected was able to serve this purpose.

The environment in the Tongue of the Ocean, a stretch of deep water in the central Bahamas, near the Berry Islands, is found to be considerably more quiescent than the energetic ambient on the east Florida shelf. TKED rates found with the VMP in this area on July 7 center around $\epsilon \approx 10^{-9}$–10^{-8} m^2 s^{-3}, with values reaching as high as 10^{-7} m^2 s^{-3} in the thermocline and 10^{-6} m^2 s^{-3} closer to the ocean surface (Fig. 8). The values from the ADVs, where all pauses were taken around 50 m depth, are higher than those of the VMP, and center around 10^{-6} m^2 s^{-3}. The estimates of ϵ_χ from the microstructure temperature data also fall within this range. The data at this station was very noisy and phase-wrapping was strong, to the point where the ADV data from the repeat occupations of this station on July 6 and July 8 were unusable. Video frames from the camera on the iMast taken during deployments revealed vibrations of the frame and/or camera housing. These vibrations may be the cause of the strong noise and excessive phase-wrapping found in the data from this station. This may also have affected the data on July 7 from which ϵ was calculated, and may have led to a high bias in the results. An alternative explanation for the high values from the ADV/CTs at this depth and station, is that the frame on which the probes were mounted caused an increase in ambient turbulence levels in this quiescent environment. The frame, as it was pulled through the water by the drifting boat, reached vertical velocities up to ∼30 cm s^{-1} and variations in depth of ∼30 cm (Fig. 3). The effect of the frame on ambient turbulence levels may have been less noticeable in the more energetic waters on the Florida shelf. Likely the strongest impact was due to the ambient atmospheric and oceanographic conditions; weather conditions on the Florida shelf were calm, yet with strong drift currents, whereas conditions during the Tongue of the Ocean deployments were breezy with significant swell, which may have contributed to cable and frame motion.

3.2. TD

Estimates of TD rates χ from the microstructure temperature probe on the iMast exhibit a similar pattern. The values largely fall within the range predicted by the VMP, except at the Bahamas station,

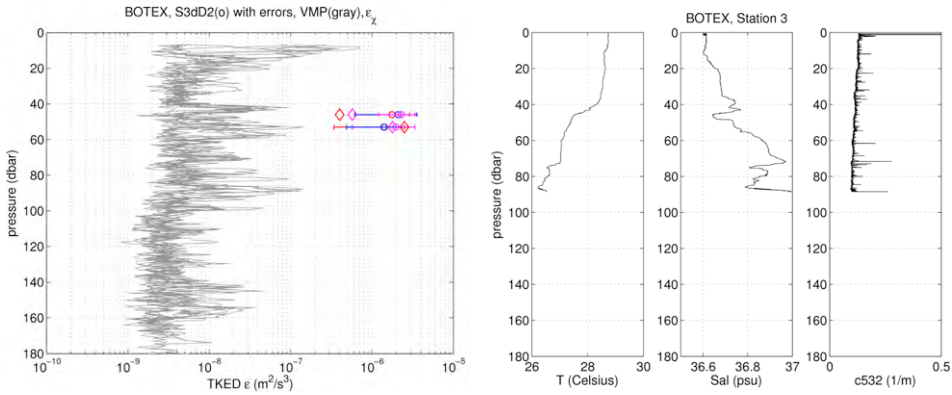

Fig. 8. TKED rates from Station 3 (Bahamas, Tongue of the Ocean) from VMP and Nortek ADV on the iMast (left). Stratification and c532 from the CTD/optics package at this station are shown on the right. The thin lines show different realizations of VMP drops for ϵ. Estimates of TKED rate ϵ from the ADV data are shown as circles with associated error bars (2 standard errors estimated via MLE technique). Individual points signify data from three different instruments, color-coded red, purple and blue. Diamonds are estimates of ϵ_χ from temperature gradient spectra from the microstructure temperature probe on the iMast.

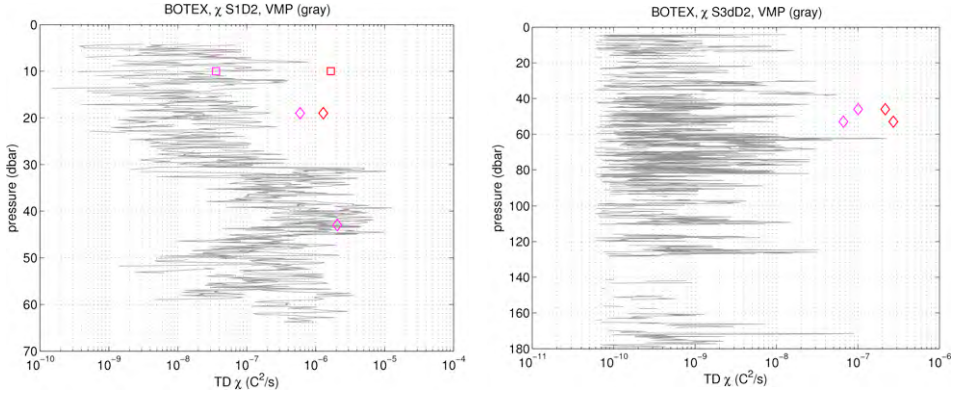

Fig. 9. TD rates from Station 1 (FL coast) and Station 3 (Bahamas, Tongue of the Ocean) from VMP and temperature microstructure probe on the iMast. The thin lines show different realizations of the VMP drops, the diamonds are TD estimates from temperature gradient spectra from the microstructure temperature probe. Squares are for a repeat realization of Station S1 (from June 30, 2011). The station was occupied on June 30 and July 2, 2011. Individual points signify data from two different instruments, color-coded red and purple.

and for the pause above the thermocline at the Florida station (Fig. 9). Especially at the Florida station, the TD rates from the VMP can be seen to show a significant increase in the thermocline, up to three orders of magnitude larger than in the well-mixed unstratified near-surface layer. The Tongue of the Ocean stations also exhibits an increase in TD near the thermocline, but it is less pronounced than at the Florida station, consistent with a much weaker thermocline near Station 3d. The values of χ from the CT data near 20 m depth in the Florida stations, which are slightly higher than those of the VMP, can be explained by the vessel drifting northwestward and onto the shelf into shallower water during deployment. The iMast data at Station 1 was taken after the VMP casts, and the drift direction of the vessel onto the narrow shelf would have led the probes to sample through an area right above the shoaling thermocline, showing increased temperature dissipation.

The estimates of χ in the Bahamas from the iMast data at around 50 m depth also show values near or above the upper bound of those seen by the VMP. The time series were taken right above

the thermocline in this area, and here, swell-induced vertical motion of the frame across layers of increased TD, or even mixing induced by the frame itself, could certainly have contributed to the slight high bias in the χ estimates. However, instrument vibration and noise contamination cannot be completely ruled out and may also have affected the estimates of χ at this station, especially since high-frequency noise was visible in these temperature time series. Nonetheless, note that the χ estimates from the microstructure temperature data in the Tongue of the Ocean, which were taken just above the thermocline, center around 10^{-7} C^2 s^{-1}, about an order of magnitude smaller than those above or near the thermocline at the Florida station, consistent with the difference in turbulence levels seen at the two stations.

3.3. Effect on optics—S_n

Since the main focus of this paper is to describe the turbulence parameters collected with the instruments on the iMast, we only briefly describe the optical measurements, which were taken to assess the effect of turbulence on image degradation. The effect of turbulence on the optical transfer function can be described as a function of TKED and TD, since the optical turbulence coefficient can be defined as $S_n \sim \chi\epsilon^{-\frac{1}{3}}$ (Hou, 2009).

S_n is a function of microstructure spatial frequency and imaging range and enters the equation for the optical transfer function (OTF) for the case of underwater imaging, which has been described as follows (Hou, 2009), accounting for path radiance, particle, and turbulence scattering

$$\begin{aligned} OTF(\Psi, r)_{total} &= OTF(\Psi, r)_{path} \cdot OTF(\Psi, r)_{particle} \cdot OTF(\Psi, r)_{turbulence} \\ &= \left(\frac{1}{1+D}\right) \cdot e^{\left(-c\,r + b\,r\,\frac{1-e^{-2\pi\theta_0\Psi}}{2\pi\theta_0\Psi}\right)} \cdot e^{\left(-S_n\Psi^{\frac{5}{3}}r\right)} \end{aligned} \tag{9}$$

where Ψ is the angular spatial frequency, r is the imaging range, D is the normalized radiance, b is the scattering coefficient, θ_0 relates to the mean scattering angle, and c is the beam attenuation coefficient for a desired wavelength. Here, we adopt this for the broad spectrum, as it only affects high-order terms (see Hou et al., 2007).

Thus, S_n is directly related to and has been derived from the parameter commonly used in the investigation of atmospheric optical turbulence, C_n^2, see Hou (2009). The units for this parameter in the literature are based on semi-empirical relations and have no clear physical meaning (Roggemann and Welsh, 1996). S_n is given with the units of rad$^{-\frac{3}{5}}$ m^{-1}, when it appears in the equation for OTF, however, when calculated as $S_n \sim \chi\epsilon^{-\frac{1}{3}}$, the units are neglected (Hou et al., 2012b). More details on S_n and its relationship to the optical transfer function can be found in Hou (2009); Hou et al. (2012b).

We estimate values of S_n for Stations 1 and 3d, in Florida and the Bahamas, respectively, for the pauses near or just above the thermocline, where we can expect the strongest optical turbulence.

At Station 1 near the Florida coast, at ~20 m depth, with a beam attenuation at 532 nm of $c532 \approx 0.15$ m^{-1}, using 532 nm as a proxy (Hou et al., 2007), the value becomes

$S_n \sim 10^{-7}$ C^2 s^{-1}$(10^{-6}$ m^2 s$^{-3})^{-\frac{1}{3}} \approx 10^{-5}$ with the VMP data, or
$S_n \sim 10^{-6}$ C^2 s^{-1}$(10^{-6}$ m^2 s$^{-3})^{-\frac{1}{3}} \approx 10^{-4}$ from ADV/CT data on the iMast (Table 1).

In the Bahamas, near 50 m depth and with a $c532 \sim 0.1$ m^{-1},

$S_n \sim 10^{-9}$ C^2 s^{-1}$(10^{-8}$ m^2 s$^{-3})^{-\frac{1}{3}} \approx 5 \times 10^{-7}$ from the VMP and
$S_n \sim 10^{-7}$ C^2 s^{-1}$(10^{-6}$ m^2 s$^{-3})^{-\frac{1}{3}} \approx 10^{-5}$ from the iMast.

The data from the iMast show higher values of χ and ϵ for both stations, which is not unexpected, given the complexities and challenges involved in interpreting the ADV data collected on a platform subject to wave motion and cable vibration (Table 1). Nonetheless, the data are able to capture the trend.

Not surprisingly, the impact of optical turbulence is found to be more pronounced in the more energetic environment near the Florida coast and less apparent in the deeper, quiescent waters in

Table 1
Optical turbulence parameter S_n.

Location	Instrument	Depth (m)	$c532$ (m^{-1})	χ (C^2 s^{-1})	ϵ(m^2 s^{-3})	S_n
FL	VMP	20	0.15	10^{-7}	10^{-6}	10^{-5}
FL	iMast	20	0.15	10^{-6}	10^{-6}	10^{-4}
Bah	VMP	50	0.1	10^{-9}	10^{-8}	$5 \cdot 10^{-7}$
Bah	iMast	50	0.1	10^{-7}	10^{-6}	10^{-5}

Table 2
Optical transfer function *OTF*.

Location	Instrument	$c532$ (m^{-1})	S_n	$OTF_{particle}$	$OTF_{turbulence}$
FL	*VMP*	0.15	10^{-5}	0.86	0.37
FL	*iMast*	0.15	10^{-4}	0.86	0.0001
Bah	*VMP*	0.10	10^{-6}	0.91	0.90
Bah	*iMast*	0.10	10^{-5}	0.91	0.37

the Tongue of the Ocean. Frames taken from the videos on the iMast confirm this finding (Figs. 10–13). Frames are shown at 10 s intervals, and illustrate the variability over the course of about 1 min, especially near the Florida coast. At the same level of magnification, the image from the Bahamas stations appears clearer, especially at high frequencies, than the image from the Florida station. Near the Florida Coast, the variability is particularly pronounced at higher spatial frequencies, indicative of the effects of turbulent density variations on the images. Note that beam c enters the equation for the optical transfer function (Eq. (9)) in the exponent, thus, while the beam c values measured at the two stations, indicative of levels of particle concentrations, differ slightly, the 0.05 m^{-1} difference in beam c cannot account for all of this image degradation. This can be seen from a simple calculation of OTFs using Eq. (9). We can choose $\theta_0 = 0.03$, $r = 1$ and $\Psi \sim 1000$, as well as $b = 0.12$ m^{-1} for Florida and $b = 0.08$ m^{-1} for the Bahamas. This will result in $OTF_{particle} = 0.86$ for a $c = 0.15$ m^{-1} as seen at the Florida station, and $OTF_{particle} = 0.91$ for a $c = 0.10$ m^{-1} as seen at the Bahamas station. The contribution of the turbulence, when calculated using the values for χ and ϵ from the VMP, comes to $OTF_{turbulence} = 0.37$ for $S_n^{VMP} = 10^{-5}$, such as at the Florida station, and $OTF_{turbulence} = 0.90$ for $S_n^{VMP} = 10^{-6}$, for the Bahamas Station. Table 2 summarizes these values. As noted previously, there are some uncertainties associated with the numbers calculated from the ADV/CT data on the frame, but the data are able to capture the general trend. It is interesting to note that, when optical turbulence is extremely high, $S_n \sim 10^{-4}$, then OTF_{turb} tends to zero for high spatial frequencies, which is in line with the Simple Underwater Imaging Model (SUIM) described in Hou (2009).

We acknowledge that the particle fields at the two locations are also likely to differ and thus affect the images, however, the detailed investigation of this influence is beyond the scope of this paper.

To quantify the extent of image degradation, including imaged degradation due to the effect of turbulence microstructure, we apply the Structural Similarity Index Method (SSIM) (Wang et al., 2004) to a subset of the images containing the higher spatial frequencies, since the effect of turbulence on image degradation is especially pronounced at higher spatial frequencies.

Here, we use images taken near the water surface, shortly after the frame enters the water and is held steady near the surface, as the respective reference images for the two stations. This also serves to effectively normalize the particle fields and ambient light conditions for the respective stations.

The SSIM values are indicated in Figs. 11 and 13 and shown as a time series in Fig. 14. They confirm that the image degradation as well as the low-frequency temporal variability, which is indicative of turbulence effects, are greater near the Florida coast. The high-frequency temporal variability and larger spread seen in the images from the Bahamas is related to vibrations of the frame, likely due to cable motion enhanced by the sea-state. These vibrations can be seen in the video images and may not be entirely removed by the shift invariance algorithm. An alternative method to the SSIM, is to calculate the SAD for subsequent image frames. The resulting time series is also shown in Fig. 14. The SAD values (normalized to the range of 0–1 and shown as $1 - SAD$) overall follow the SSIM, however, there appears to be increased high-frequency variability in the Bahamas station, especially

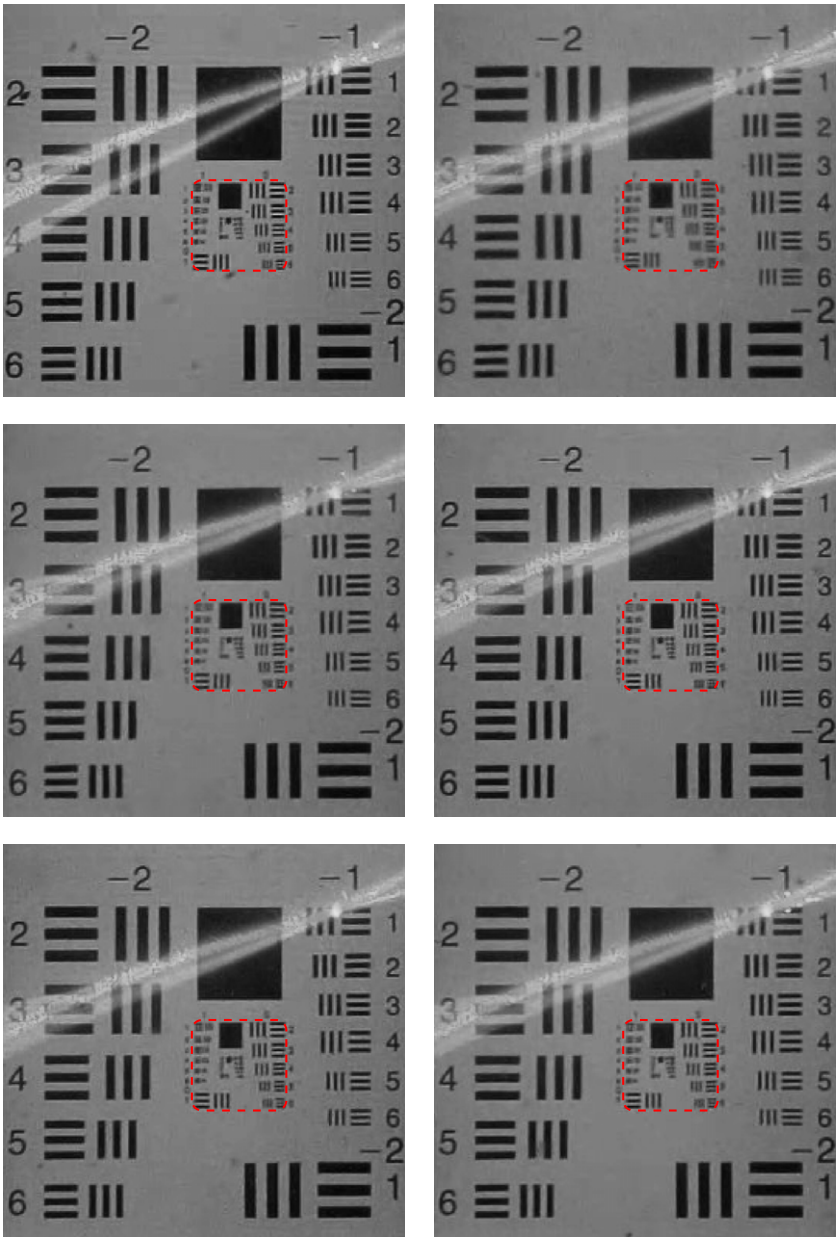

Fig. 10. Frames from the HS video taken on the iMast near the Florida coast (Station S1 at 20 m depth; resolution 512 by 384 pixels at 300 fps) are shown at 10 s intervals (time progression is from left to right and top to bottom, starting with top right image). Reference image is shown on the top left. The dashed rectangle indicates the part of the image that is shown in more detail in Fig. 11.

towards the beginning of the time series. This can be attributed to the aforementioned high-frequency vibrations seen in the images from this station. Any lateral shift in the image, such as caused by vibrations will lead to a high value of SAD, whereas turbulence, which leads to the deformation of adjacent pixels, will be better detected by the SSIM algorithm.

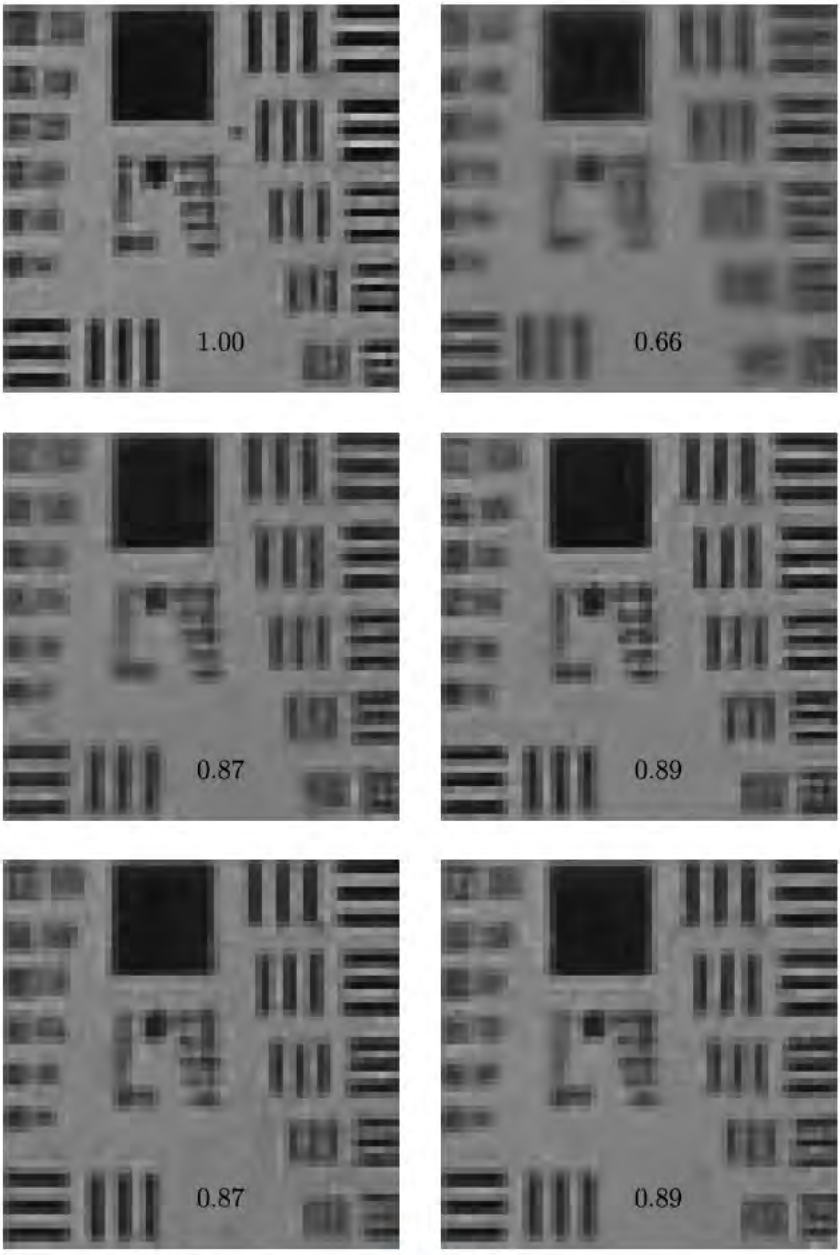

Fig. 11. Close-up of the area of the dashed rectangle from Fig. 10 highlights the variability at higher spatial frequencies, at 10 s intervals (time progression is from left to right and top to bottom, starting with image on top right). The black numbers are the values from applying the SSIM algorithm to these images using a reference image (top left) from near the surface at this location.

4. Summary and discussion

In order to test a new platform to study the impact of oceanic optical turbulence on EO signal transmission, we collected high-resolution velocity and temperature data along with high-resolution

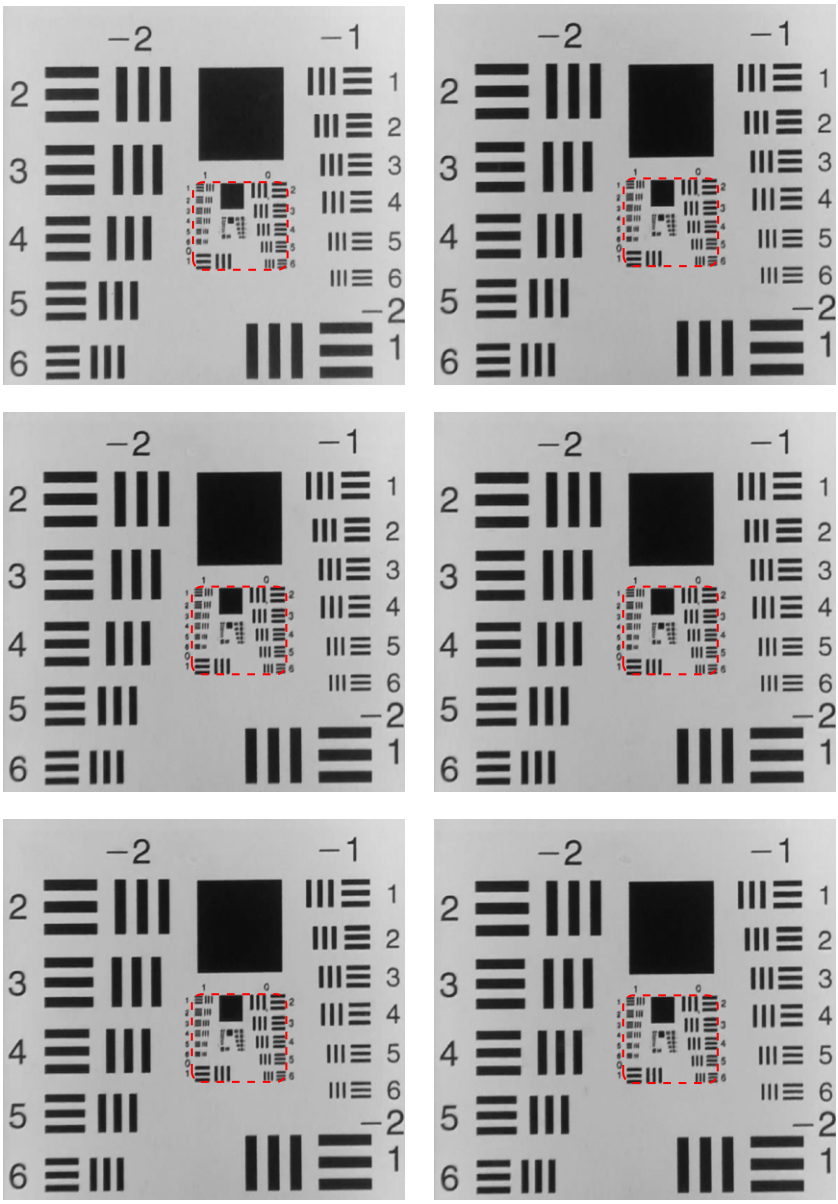

Fig. 12. Frames from the HD video taken on the iMast in the Bahamas (Station S3 at 50 m depth; resolution 1920 by 1080 pixels at 60 fps) are shown at 10 s intervals (time progression is from left to right and top to bottom, starting with top right image). Reference image is shown on the top left. The dashed rectangle indicates the part of the image that is shown in more detail in Fig. 13.

video frames in the waters off the Florida coast and the Bahamas. A VMP was deployed to collect profiles of velocity shear and temperature data. TKED and TD rates were inferred from the ADV and temperature microstructure data, compared to the dissipation rates from the VMP and put into the context of the optical measurements.

There are considerable inherent challenges to the study of optical turbulence in the open ocean. The temporal and spatial scales are vastly different between the quasi-instantaneous optical

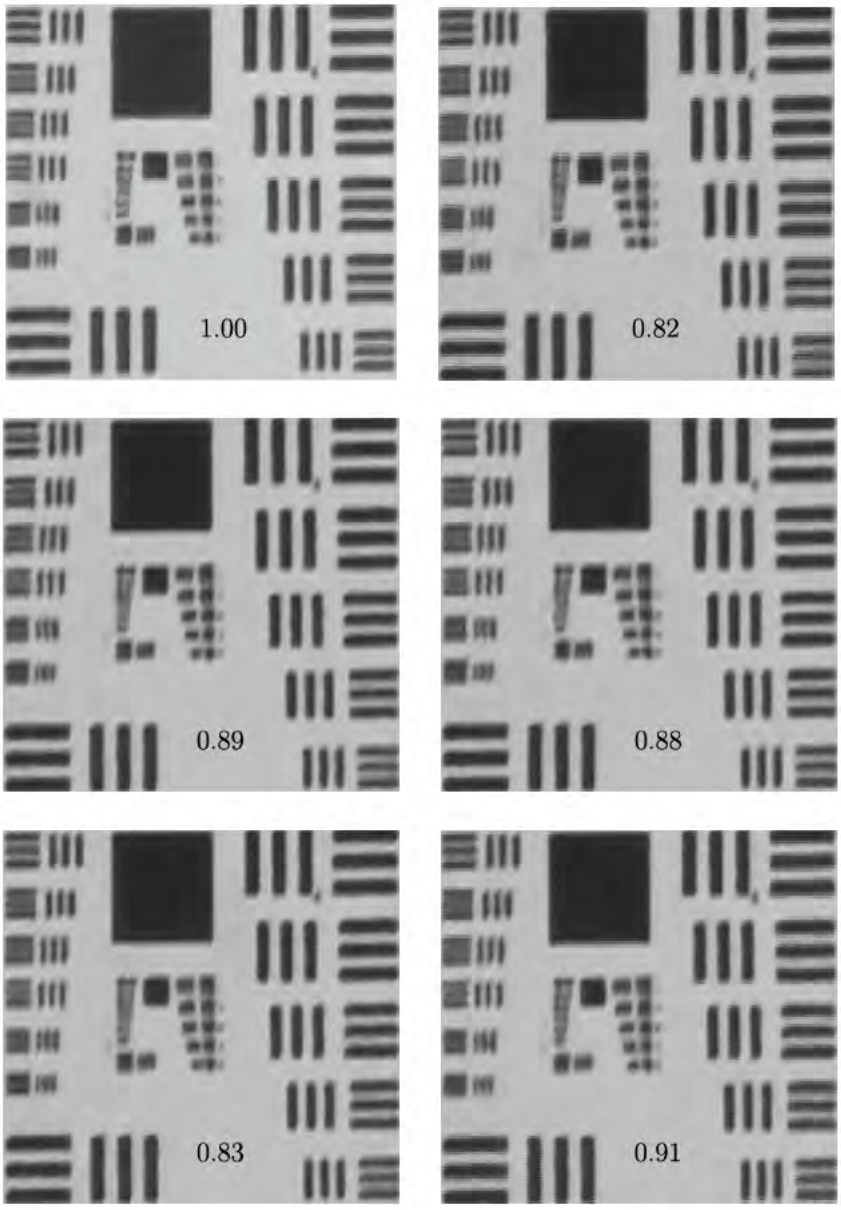

Fig. 13. Close-up of the area of the dashed rectangle from Fig. 12, at 10 s intervals (time progression is from left to right and top to bottom, starting with image on top right). The black numbers are the values from applying the SSIM algorithm to these images (using a reference image from near the surface at this location, shown on top left) and show less variability than in Fig. 11.

measurements (on the order of ms) and the statistical averages needed for velocity and temperature data to estimate turbulence properties (on the order of tens of minutes). This scale discrepancy is compounded by the temporal and spatial variability of oceanic turbulence, which is well-known to be intermittent and "patchy".

Measuring turbulence in the ocean is a challenging task, complicated by deployment strategy, apparent in our data as the drift across a shoaling thermocline on the Florida shelf, and likely frame-

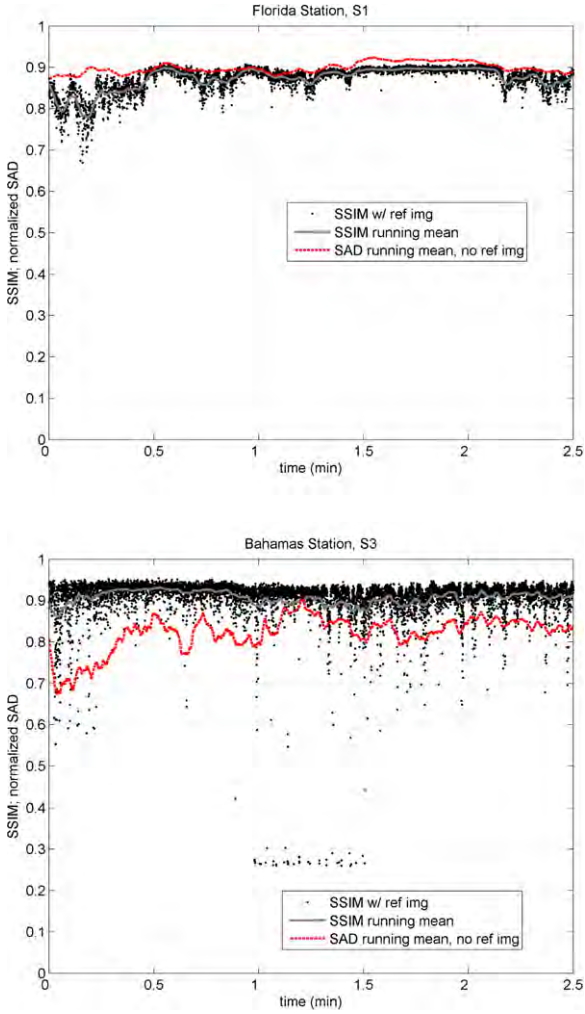

Fig. 14. Time series of the SSIM algorithm applied to video stills from near the Florida Coast (top) and the Bahamas (bottom) over several minutes illustrate the variability in image degradation at both locations. The gray line shows the running mean of the two time series. The low-frequency temporal variability and the image degradation are more pronounced near the Florida Coast. The dashed red line shows the running mean of the sum of absolute differences (SAD) for subsequent video frames in the time series. The value of SAD is scaled to fit into the range 0–1 and shown as $1 - SAD$. (For interpretation of the references to color in this figure legend, the reader is referred to the web version of this article.)

induced turbulence in the Bahamas, as well as the ambient environmental conditions of ocean and atmosphere. Furthermore, the use of ADVs to infer TKED is inherently more successful in more energetic environments, such as that encountered on the Florida shelf. In the calmer waters of the Tongue of the Ocean, Bahamas, the signal to noise ratio of the sensor may get close to its lower limit. The noise from platform motion and vibrations, apparent mainly in our velocity data, can further complicate the estimation of turbulence properties from the ADV/CT package. Thus, complementary measurements of ambient turbulence levels with a dedicated microstructure profiler, such as the VMP, are an invaluable tool to aid in data analysis and guide error estimates.

Despite these difficulties, the data from ADV and temperature microstructure probe were able to provide information on the turbulence experienced by the iMast, while simultaneously collecting information on the impact of this turbulence on image degradation. Increased levels of optical turbu-

lence were expected to be found above or near the thermocline and these optical turbulence levels predicted by the VMP and ADV/CT data were confirmed by the images taken during the iMast deployments. This study was the first comprehensive effort collecting data from both a traditional profiling approach for measuring turbulence, as well from an ADV/CT package on a moving platform, for the investigation of optical turbulence in the energetic open ocean environment.

While there are many challenges, the effort of studying optical turbulence in the natural environment is necessary to quantify the impact of oceanic microstructure on underwater EO signal transmission and to advance our knowledge on the use of optical techniques to measure turbulence. Future field studies of optical turbulence may benefit from a platform design that allows the frame to freely drift or fall through the water column, while still maintaining an adequate optical path length.

The results of our study will help address the sampling challenges for future field efforts aimed at quantifying optical turbulence and may also improve our understanding of the use of ADVs to probe oceanic turbulence. In addition to studies of naturally-occurring optical turbulence, laboratory experiments, conducted in a controlled laboratory environment and complemented by numerical simulations, should prove very useful to the detailed and quantitative investigation of the processes involved in optical turbulence in the ocean.

Acknowledgments

We would like to thank Drs. Danielle Wain, Cynthia Bluteau and Barry Ruddick for sharing their respective Matlab scripts for the calculation of TKED and TD rates, parts of which we incorporated in our own processing routines. The captain and crew of the R/V Walton Smith are gratefully acknowledged. We thank Dr. Clare Reimers and UNOLS for awarding S. Matt participation in the 2012 UNOLS training cruise and for helpful discussions, which directly benefited the analysis of the data presented here. Joshua Xu is acknowledged for his help with video and data processing. We thank two anonymous reviewers for their comments, which improved the manuscript. This work was supported by ONR program element 62782N. Silvia Matt was supported by a National Research Council Research Associateship.

References

Bluteau, C.E., Jones, N.L., Ivey, G.N., 2011. Estimating turbulent kinetic energy dissipation using the inertial subrange method in environmental flows. Limnol. Oceanogr. Methods 9, 302–321.
Bogucki, D.J., Domaradzki, J.A., Ecke, R.E., Truman, C.R., 2004. Light scattering on oceanic turbulence. Appl. Opt. 43, 5662–5668.
Bogucki, D.J., Domaradzki, J.A., Stramski, D., Zaneveld, J.R., 1998. Comparison of near-forward light scattering on oceanic turbulence and particles. Appl. Opt. 37, 4669–4677.
Bogucki, D.J., Luo, H., Domaradzki, J.A., 2012. Experimental evidence of the Kraichnan scalar spectrum at high Reynolds numbers. J. Phys. Oceanogr. 42, 1717–1728.
Dalgleish, F., Hou, W., Vuorenkoski, A., Nootz, G., Ouyang, B., 2013. In situ laser sensing of mixed layer turbulence. Proc. SPIE 8724, http://dx.doi.org/10.1117/12.2019193. 87240D–87240D–12.
Duntley, S.Q., 1963. Light in the sea. J. Opt. Soc. Amer. 53, 214–233.
Hou, W., 2009. A simple underwater imaging model. Opt. Lett. 34, 2688–2690. http://dx.doi.org/10.1364/OL.34.002688.
Hou, W., Jarosz, E., Dalgleish, F., Nootz, G., Woods, S., Weidemann, A.D., Goode, W., Vuorenkoski, A., Metzger, B., Ramos, B., 2012a. Bahamas optical turbulence exercise (BOTEX): preliminary results. Proc. SPIE 8372, http://dx.doi.org/10.1117/12.920740. 837206–10.
Hou, W., Lee, Z., Weidemann, A.D., 2007. Why does the secchi disk disappear? An imaging perspective. Opt. Express 15, 2791–2802.
Hou, W., Woods, S., Jarosz, E., Goode, W., Weidemann, A., 2012b. Optical turbulence on underwater image degradation in natural environments. Appl. Opt. 51, 2678–2686.
Lesieur, M., 2008. Turbulence in Fluids, fourth ed.. Springer.
Moum, J., Nash, J., 2009. Mixing measurements on an equatorial ocean mooring. J. Atmos. Ocean. Technol. 26, 317–336.
Nash, J.D., Moum, J.N., 1999. Estimating salinity variance dissipation rate from conductivity microstructure measurements. J. Atmos. Ocean. Technol. 16, 263–274.
Oakey, N.S., 1982. Determination of the rate of dissipation of turbulent energy from simultaneous temperature and velocity shear microstructure measurements. J. Phys. Oceanogr. 12, 256–271.
Preisendorfer, R.W., 1986. Secchi disk science: visual optics of natural waters. Limnol. Oceanogr. 31, 909–926.
Roggemann, M.C., Welsh, B.M., 1996. Imaging through Turbulence. CRC Press, Boca Raton, Florida, USA.
Ruddick, B., Anis, A., Thompson, K., 2000. Maximum likelihood spectral fitting: the batchelor spectrum. J. Atmos. Ocean. Technol. 17, 1541–1555.
Rusello, P.J., 2009. A practical primer for pulse coherent instruments, Nortek Technical Note TN-027. pp. 1–17.

Rusello, P., Cowen, E., 2011. Turbulent dissipation estimates from pulse coherent doppler instruments. In: 10th IEEE/OES Current, Waves and Turbulence Measurements, CWTM, pp. 167–172.
Tennekes, H., Lumley, J.L., 1972. A First Course in Turbulence. MIT Press.
Wang, Z., Bovik, A.C., Sheikh, H.R., Simoncelli, E.P., 2004. Image quality assessment: from error visibility to structural similarity. IEEE Trans. Image Process. 13, 600–612.
Wolk, F., Yamazaki, H., Seuront, L., Lueck, R.G., 2002. A new free-fall profiler for measuring biophysical microstructure. J. Atmos. Oceanic Technol. 19, 780–793.
Woods, S., Hou, W., Goode, W., Jarosz, E., Weidemann, A., 2011. Quantifying turbulence microstructure for improvement of underwater imaging. Proc. SPIE 8030, http://dx.doi.org/10.1117/12.887607. 80300A–11.